Temporal codes of visual working memory in the human cerebral cortex: Brain rhythms associated with high memory capacity

Noguchi, Yasuki

Kakigi, Ryusuke

(Citation)
NeuroImage, 222:117294-117294

(Issue Date)
2020-11-15

(Resource Type)
journal article

(Version)
Version of Record

NeuroImage 222 (2020) 117294

Contents lists available at ScienceDirect

NeuroImage

journal homepage: www.elsevier.com/locate/neuroimage

Temporal codes of visual working memory in the human cerebral cortex Brain rhythms associated with high memory capacity

Yasuki Noguchi [1,*], Ryusuke Kakigi [2]

[a] Department of Psychology, Graduate School of Humanities, Kobe University, 1-1 Rokkodai-cho, Nada, Kobe, 657-8501, Japan
[b] Department of Integrative Physiology, National Institute for Physiological Sciences, 38 Nishigonaka, Myodaiji, Okazaki, 444-8585, Japan

ARTICLE INFO

Key words:
Magnetoencephalography
Change detection
Alpha frequency
Beta frequency
Front-parietal cortex

ABSTRACT

Visual working memory (vWM) is an important ability required for various cognitive tasks although its neural underpinnings remain unclear. While many studies have focused on theta (4–7 Hz) and gamma (> 30 Hz) rhythms as a substrate of vWM, here we show that temporal signals embedded in alpha (8–12 Hz) and beta (13–30 Hz) bands can be a good predictor of vWM capacity. Neural activity of healthy human participants was recorded with magnetoencephalography when they performed a classical vWM task (change detection). We analyzed changes in inter-peak intervals (IPIs) of oscillatory signals along with an increase in WM load (a number of to-be-memorized items, 1–6). Results showed a load-dependent reduction of IPIs in the parietal and frontal regions, indicating that alpha/beta rhythms became faster when multiple items were stored in vWM. Furthermore, this reduction in IPIs was positively correlated with individual vWM capacity, especially in the frontal cortex. Those results indicate that vWM is represented as a change in oscillation frequency in the human cerebral cortex.

1. Introduction

Working memory (WM) is a fundamental ability in various cognitive skills, such as goal-directed behaviors, inference, calculations, and decision making (Baddeley, 2012; D'Esposito and Postle, 2015; Eriksson et al., 2015; Jacob et al., 2018; Kaminski et al., 2017; Leavitt et al., 2017; Luck and Vogel, 2013; Ma et al., 2014). Although its neural mechanisms remain a matter of debate (Constantinidis et al., 2018; Lundqvist et al., 2018; Stokes, 2015), an increasing number of studies have reported a close relationship of WM with oscillatory signals in the brain (Johnson et al., 2017; Kornblith et al., 2016; Roux and Uhlhaas, 2014). Especially, a model based on the cross-frequency coupling between theta (4–7 Hz) and gamma (> 30 Hz) rhythms has gained much attention (Axmacher et al., 2010; Canolty et al., 2006; Lisman and Jensen, 2013; Miller et al., 2018; Reinhart and Nguyen, 2019; Sauseng et al., 2009).

In contrast to the theta and gamma rhythms, a role of alpha (8–12 Hz) and beta (13–30 Hz) rhythms in WM is relatively unknown, partly because those rhythms are thought to reflect a suppression of neural processing (Jensen and Mazaheri, 2010; Shin et al., 2017; van Ede et al., 2011). Several studies reported an increase in power of alpha and beta bands during a retention period of vWM task (Jensen et al., 2002; Palva et al., 2011; Wianda and Ross, 2019). Of particular interest was an intermediate frequency between alpha and beta (12–15 Hz, called the upper-alpha or lower-beta rhythm) (Palva et al., 2011; Wianda and Ross, 2019) whose amplitudes were modulated by memory loads and further predicted individual WM capacity. Although those studies consistently showed an involvement of alpha/beta rhythms in vWM, their functional role remains still unclear. While some studies indicated a facilitatory role of alpha/beta activity in WM maintenance (Bonnefond and Jensen, 2012; Gelastopoulos et al., 2019; Spitzer and Haegens, 2017), others not (Mapelli and Ozkurt, 2019; Proskovec et al., 2018).

Most studies listed above have investigated changes in power (amplitude) of alpha/beta rhythm related to vWM. Here we address this issue by measuring a *speed* of those waves, using the inter-peak interval (IPI) analysis of magnetoencephalography (MEG) (Noguchi et al., 2019). In this analysis, raw waveforms of MEG are filtered with a passband of interest (e.g. 8–30 Hz for alpha-to-beta band). Each interval between contiguous peaks in the filtered waveforms is defined as IPI (**Fig. 1A**). Changes in mean IPI lengths indicate changes in oscillation frequency (speed) of alpha/beta waves (faster rhythm produces shorter IPIs, **Fig. 1B**). This approach focusing on temporal codes of oscillatory signals might reveal a new role of alpha/beta rhythms in vWM.

One advantage of our IPI analysis is that it can evaluate not only speed but also the *regularity* of brain rhythms; a smaller variance of an IPI distribution indicates higher regularity of oscillatory signal (**Fig. 1C**). Here we use this approach to test the "attractor hypothesis" in WM.

* Correspondence should be addressed to Yasuki Noguchi, Department of Psychology, Kobe University, 1-1 Rokkodai-cho, Nada, Kobe, 657-8501, Japan,
E-mail address: ynoguchi@lit.kobe-u.ac.jp (Y. Noguchi).

https://doi.org/10.1016/j.neuroimage.2020.117294
Received 4 May 2020; Received in revised form 15 August 2020; Accepted 18 August 2020
Available online 21 August 2020

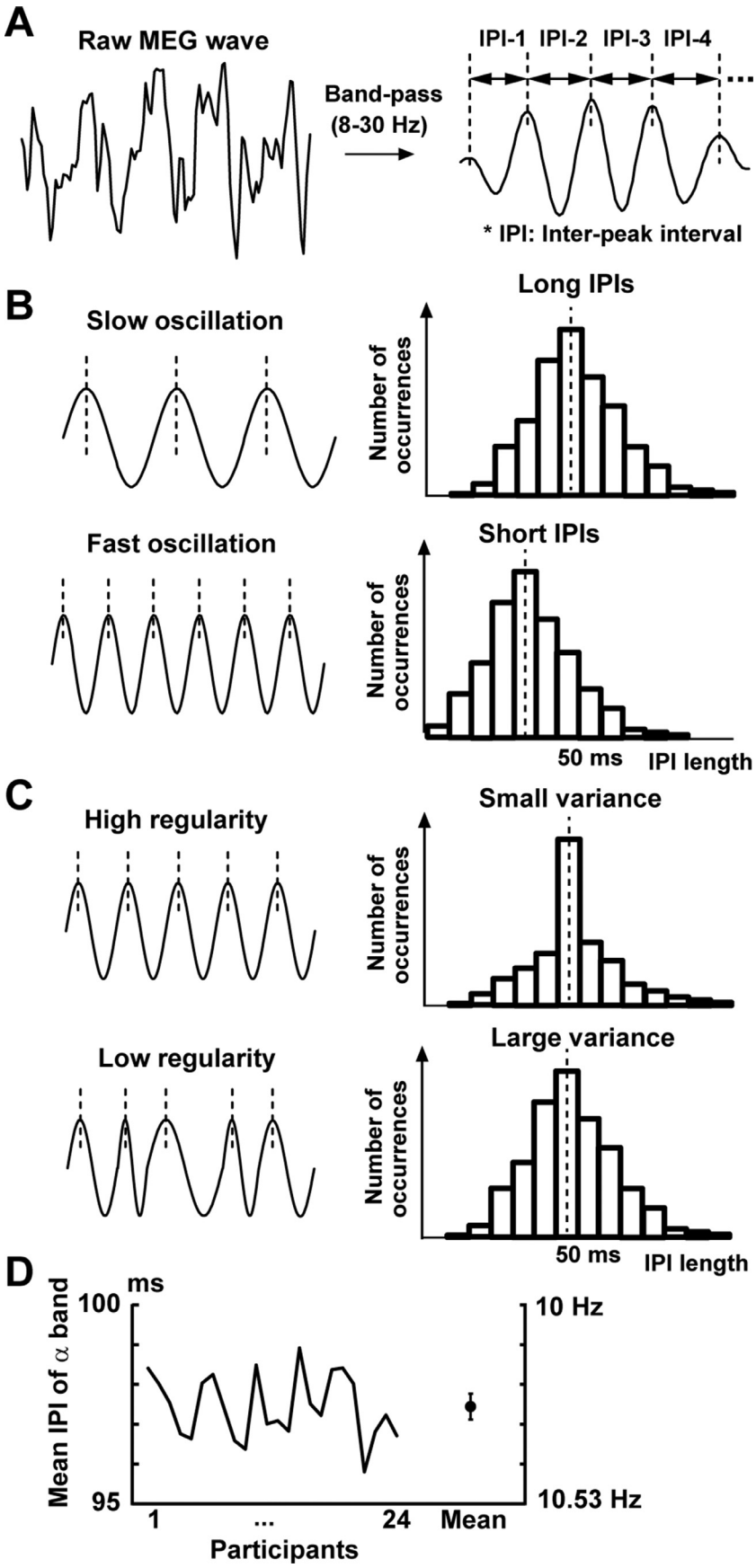

Fig. 1. Schematic illustrations of the inter-peak interval (IPI) analysis. We first extracted oscillatory signals at a frequency band of interest, e.g. alpha-to-beta band (8–30 Hz), with a band-pass filter (**A**). Each IPI was measured as a time length between two peaks of the filtered waveform. We then pooled all IPIs within a retention period (300 – 900 ms, Fig. 2) across trials, depicting a distribution of their occurrences. Since slow/fast oscillatory signals produce longer/shorter IPIs, changes in oscillation frequency can be measured as changes in mean IPIs (**B**). On the other hand, the regularity of oscillatory signals can be indexed by a variance of the IPI distribution (**C**), because an irregular signal produces many IPIs distant from the mean. Panel (**D**) shows individual data of mean IPI in a baseline period (−1300 to −700 ms, Fig. 2) identified with a band-pass filter of 8 – 12 Hz (alpha band). A black dot and error bar show a mean and 95% confidence interval over 24 participants.

Although there is an intense debate about neural underpinnings of WM, electrophysiological studies on animals have proposed the attractor states (stable fixed points in collective neuronal activity) as a key mechanism for memory retention (Brody et al., 2003; Chaudhuri and Fiete, 2016; Compte et al., 2000; Inagaki et al., 2019; Murray et al., 2017). We expect that those attractor states might be measured as a reduced variance of IPIs, because they emerge from a self-sustained recurrent neural network (Macoveanu et al., 2006; Standage and Pare, 2018; Wimmer et al., 2014) that can generate periodic (regular) signals. Such data would provide further evidence for the attractor hypothesis, elucidating neural substrates of WM in the normal human brain.

2. Materials and methods

2.1. Participants

Twenty-four healthy human subjects with normal or corrected-to-normal vision participated in the present study. This sample size was based on the power analysis using G*Power 3 (Faul et al., 2007). An effect size was estimated from data of our previous MEG study (Noguchi et al., 2019), with the type I error rate (alpha) and statistical power (1 - beta) set at ⟨ 0.05 and ⟩ 0.80, respectively. Because the data of three participants contained excessive noise in MEG waveforms (a peak-to-peak variation of > 4500 fT/cm in more than half of trials, due to dental treatments), they were discarded and replaced by those of additional three subjects. An age distribution of 24 participants (18 females) after the replacement was as follows: 1 in late 10 s (female), 17 in 20 s (11 females), 1 in 30 s (female), 4 in 40 s (4 females), and 1 in 50 s (female). None of the participants had a history of neurological disorders or took psychotropic medications. Informed consent was received from each participant after the nature of the study had been explained. All experiments were carried out in accordance with regulations and guidelines approved by the ethics committee of Kobe University, Japan.

2.2. Stimuli and task

We measured vWM capacity of the participants using a cued change-detection task (Vogel and Machizawa, 2004). All visual stimuli were generated with the Matlab Psychophysics Toolbox (Brainard, 1997; Pelli, 1997) and projected on a screen at a refresh rate of 60 Hz. Each trial started with a black fixation point (0.18 × 0.18 deg) over a gray background for 800 ms. To direct attention of participants, a cue stimulus (an arrow pointing leftward or rightward, 1.34 deg) was presented over the central field for 33 ms (**Fig. 2A**), followed by another fixation period of 467 ms. Participants then viewed a bilateral array of colored squares (memory array, 150 ms). The array consisted of 1, 2, 4, or 6 squares with different colors (memory items) in each hemifield (the numbers of squares were always the same between two hemifields). They were presented over two invisible rectangular regions of 3.89 (W) × 6.81 (V), one to the left and another to the right of the fixation point (center-to-center distance: 3.4 deg). A size of each square was 0.73 × 0.73 deg, and its color was randomly chosen from 9 colors (red, green, blue, yellow, magenta, cyan, orange, black, and white). Positions of squares were also randomized on each trial, with the constraint that a distance between squares was 1.94 deg or longer. We asked participants to remember the items in a hemifield indicated by the cue (left or right). After a retention period of 1050 ms, their memory was tested by another array (test array) that was identical to the memory array (no-change trials) or differed by one color (change trials). Participants attended to the cued hemifield and pressed one of two buttons to indicate whether the two arrays were the same ("no-change" response) or not ("change" response). They were also instructed to ignore all items in the uncued hemifield. No time limitation was imposed for the button press.

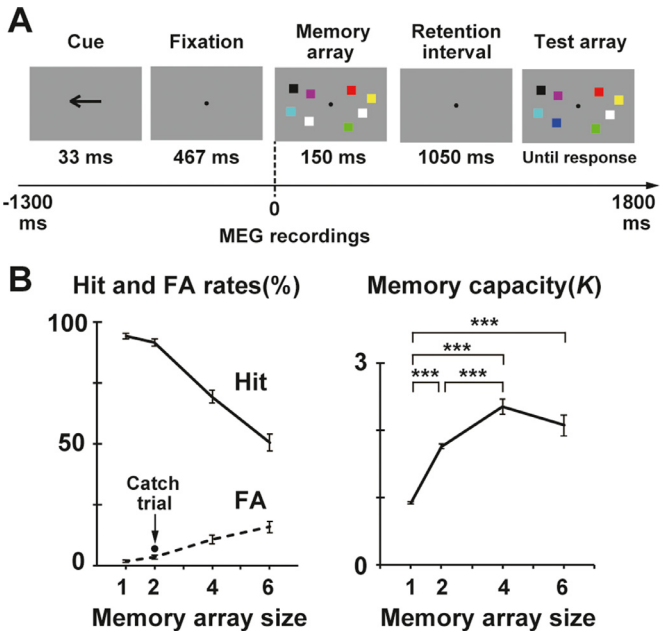

Fig. 2. Stimuli and task. (**A**) The cued change-detection task. Participants directed their attention to a cued hemifield (left of right, guided by an arrow at the beginning of each trial) and compared two arrays of colored squares (memory and test arrays) separated by a retention interval. The test array was either identical to the memory array (no-change trials) or differed by one color (change trials). Participants answered whether the two arrays were the same ("no-change" response) or not ("change" response). (**B**) Changes in task performance as a function of memory array size (numbers of to-be-memorized items, 1, 2, 4, or 6). A left panel shows hit rates (solid line) in which participants answered "change" in the change trials and false-alarm (FA) rates (dotted line) in which they answered "change" in the no-change trials. A filled black circle indicates a rate of "change" response in catch trials (see texts) where a color change occurred in an uncued hemifield. The right panel shows an index of memory capacity (*K*) estimated from the hit and FA rates (see texts for details). In this and subsequent figures, all error bars denote standard error (SE) across participants. *** $p < 0.001$.

A combination of cued hemifield (left or right) and memory array size (WM load, 1, 2, 4, or 6) produced 8 types of trials. We called the trials with leftward cue and 1 memory item as L1, while trials with rightward cue and 6 memory items were named as R6. In addition to those 8 conditions, we introduced 9th condition (catch trials) to check whether participants switched their attention following the cue. In those catch trials, two squares were presented in each hemifield. Although a color change normally took place in the cued hemifield, it occurred in the uncued hemifield in the catch trials (participants thus should press "no-change" button). If participants did *not* allocate their attention following the cue, this would be detected as a high rate of reporting "change" in the catch trials.

An experimental session comprised 100 trials in which 4 catch trials were randomly intermixed with the 96 non-catch trials (L1, L2, L4, L6, R1, R2, R4, and R6, 12 trials for each). A ratio of the change: no-change trials in the non-catch trials was 1:1. Each participant underwent 6 sessions.

Behavioral data were analyzed conforming to previous procedures. For each size of memory array (1, 2, 4, or 6), we computed a hit rate in which participants answered "change" in the change trials and a false-alarm (FA) rate in which they reported "change" in the no-change trials (**Fig. 2B**, left). Visual memory capacity of each participant (*K*, **Fig. 2B**, right) was then estimated using a formula below (Cowan, 2001; Pashler, 1988),

$$K = S \times (H - F),$$

where K is the memory capacity, S is the size of memory array, H and F are the hit and FA rates for that array size, respectively. Previous data showed that the K monotonically increased up to memory size 4, reaching a plateau of 2.5 – 3 for higher sizes (Fukuda et al., 2015; Vogel and Machizawa, 2004).

2.3. MEG recordings and preprocessing

Neural activity was measured with a whole-head MEG system (Vector-view, ELEKTA Neuromag, Helsinki, Finland) in National Institute for Physiological Sciences, Okazaki, Japan. This system recorded neural signals at 102 positions over the scalp using 204 planer-type sensors (two sensors at each recording position). One sensor measured changes of neuromagnetic signals in a latitudinal direction while the other measured changes in a longitudinal direction (sampling rate: 4000 Hz, analogue band-pass filter: 0.1 – 330 Hz). Data from those two types of sensors were integrated in later analyses (see below). Neuromagnetic waveforms measured by those planar-type gradiometers reflect neural activity in the cerebral cortex just below a recording position.

Before MEG measurements, we placed five head position indicator coils over the scalp of participants, to record their head locations with respect to MEG sensors. Locations of three anatomical landmarks (nasion and bilateral preauricular points) were also measured with a three-dimensional digitizer.

The preprocessing of MEG data was performed using the Brainstorm toolbox for Matlab (Tadel et al., 2011). Noises in waveforms caused by eye blinks and body movement were checked by visual inspection and removed through the ICA (independent component analysis) procedures implemented in the Brainstorm. Neuromagnetic waveforms were then segmented and classified into the 9 conditions above (L1, L2, L4, L6, R1, R2, R4, R6, and catch). An epoch for the segmentation was from −1300 to 1800 ms relative to an onset of a memory array (**Fig. 2A**). Trials in which a signal variation (a max-min difference within a period of −700 to 1200 ms) was larger than 4500 fT/cm were excluded from further analyses. Numbers of trials (mean ± SD across participants) after the exclusion were 64.5 ± 5.7 (L1), 63.9 ± 5.3 (L2), 65.3 ± 5.0 (L4), 65.2 ± 4.8 (L6), 64.5 ± 5.0 (R1), 64.1 ± 5.1 (R2), 64.3 ± 6.2 (R4), and 63.5 ± 5.5 (R6). A two-way ANOVA of memory field (left/right) and WM load (1/2/4/6) on those numbers of trials indicated no main effect (memory field: $F(1,23) = 2.88$, $p = 0.10$, $\eta^2 = 0.111$, WM load: $F(3,69) = 0.88$, $p = 0.46$, $\eta^2 = 0.037$) or interaction ($F(3,69) = 1.54$, $p = 0.21$, $\eta^2 = 0.063$).

2.4. Power analysis

We first analyzed changes in power of oscillatory signals over time (**Fig. 3**). Using the time-frequency (TF) analysis in the Brainstorm, we converted MEG waveforms into power spectra of time (−1300 to 1800 ms) × frequency (1 to 100 Hz). Those TF spectra were averaged across trials and between longitudinal and latitudinal sensors at each recording position. We then performed a baseline correction of the TF data. For each frequency, all data at −1300 to 1800 ms were converted into decibel (dB) change from a baseline (pre-cue period, −700 to −500 ms), as shown by an equation below.

$$y = 10 \times \log 10(x/u)$$

, where x and y indicate powers before and after the conversion, and u indicates a mean power in the baseline period.

2.5. Inter-peak interval analysis

Speed and regularity of oscillatory signals were evaluated by the IPI analysis. First, a raw MEG waveform was decomposed into 5 frequency bands (delta: 2–4 Hz, theta: 5–7 Hz, alpha/beta: 8–30 Hz, gamma: 31–59 Hz, and high-gamma: 61–100 Hz) with band-pass filters. For each

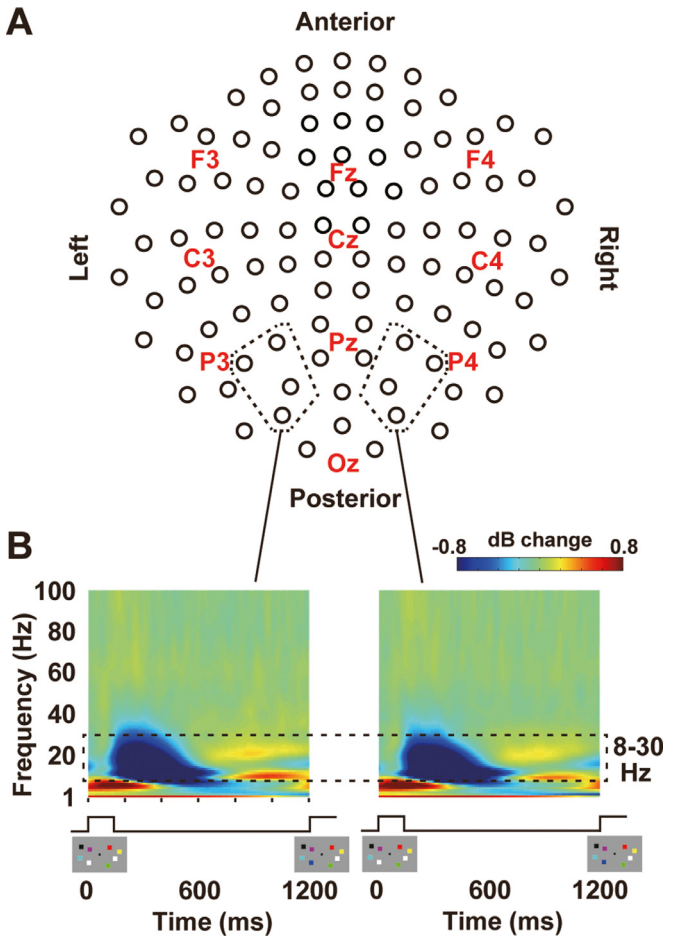

Fig. 3. Changes in power of oscillatory signals over the prieto-occipital regions. (**A**) A two-dimensional array of MEG sensors at 102 locations over the scalp. Approximate positions are indicated by labels in the international 10–20 system (e.g. Cz). (**B**) Time-frequency (TF) spectra. Data at four sensor positions over the occipito-parietal regions were averaged for each hemisphere. Oscillatory signals in the alpha-to-beta band (8–30 Hz, shown by a dotted rectangle) showed prominent decrease in power at 200 – 600 ms, which was followed by a weak increase after 600 ms.

of the 5 filtered waveforms, we measured intervals between contiguous peaks (IPIs). All IPIs during a memory retention period, i.e. 300 - 900 ms from an onset of memory array (Vogel and Machizawa, 2004), were pooled across trials and between latitudinal and longitudinal sensors. This procedure generated a distribution of IPIs (**Fig. 1B**) at each recording position in each condition. Finally, we computed three parameters of the IPI distribution; mean, standard deviation (SD), and coefficient of variation (CV). The CV was obtained by dividing the SD of IPIs by their mean (CV = SD/mean). It has been used as an index of irregularity (variability) of neural signals (Compte et al., 2003; Qi and Constantinidis, 2015; Standage and Pare, 2018). A higher CV indicates lower regularity of signals.

2.6. Statistical procedures

We first explored the IPI changes related to WM by comparing two types of trials; Memorize-Left trials (L1 – L6) in which participants memorized items in the left hemifield and Memorize-Right trials (R1 – R6) in which they memorized items in the right hemifield. As shown in the left panel of **Fig. 4A**, mean IPIs of 8–30 Hz at right posterior sensors became shorter than those at left posterior sensors in Memorize-Left trials, while retaining items in the right hemifield reduced IPI at the left posterior sensors (middle panel). Contrasting the Memorize-Left and Memorize-

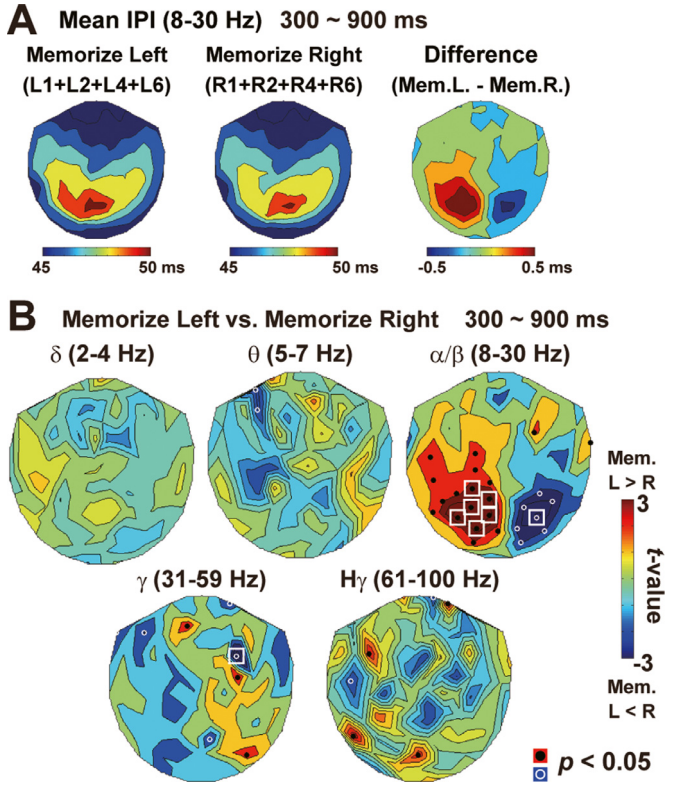

Fig. 4. Changes in mean IPIs during the retention period (300 – 900 ms). (**A**) Contour maps of mean IPI over the 102 locations. The left map shows mean IPIs at alpha-to-beta band (8 – 30 Hz) when participants memorized 1–6 items in left hemifield (L1 – L6), while the middle map shows those when they memorized right hemifield (R1 – R6). A differential map (L1+L2+L4+L6 vs. R1+R2+R4+R6) in the right panel depicts posterior brain regions showing shorter IPIs when items in contralateral hemifield were retained. (**B**) The *t*-maps of mean IPIs (L1+L2+L4+L6 vs. R1+R2+R4+R6) at five frequency bands from delta (2 – 4 Hz) to high-gamma (61 – 100 Hz). Black dots and white circles denote sensor positions showing a significant ($p < 0.05$, uncorrected) difference. White rectangles indicate a significant difference after a correction of multiple comparisons (see texts). The laterality of retention-related decrease in IPIs was most clearly observed at 8 – 30 Hz.

Right conditions (right panel) thus isolated hemisphere-specific neural activity related to WM maintenance with total visual inputs in bilateral hemifields equated between conditions. Statistical *t*-maps are shown in **Fig. 4B**. Since a paired *t*-test ($N = 24$ vs. 24) was repeated for 102 sensor positions, we resolved a problem of multiple comparisons by controlling false discovery rate (FDR). A statistical threshold was adjusted with Benjamini-Hochberg correction (Benjamini and Hochberg, 1995) by setting the *q*-value at 0.05. Sensors showing a significant difference after this correction were marked with white rectangles in **Fig. 4B**.

Another hallmark of memory-related neural activity is load-dependent changes. We checked this point by contrasting Memorize-Left and Memorize-Right trials for each memory load (L1 vs. R1 and L2 vs. R2, etc. **Fig. 5A**). If the IPI changes reflected an amount of information stored in memory, the contrast would be clearer as an increase of memory load (Vogel and Machizawa, 2004). To highlight a difference between sub-capacity conditions (when memory array size was smaller than the limit of vWM capacity, 2.5 – 3) and supra-capacity conditions (when memory array size was larger than the limit), we made the same comparison by averaging the data in loads 1 and 2 (L1+L2 vs. R1+R2, low-load condition) and by averaging the data in loads 4 and 6 (L4+L6 vs. R4+R6, high-load condition). The sensors showing a significant difference (after the FDR correction) in either the low- or high-load condition were defined as the sensors of interest (SOIs). Finally, IPI data were averaged across SOIs for each hemisphere and submitted to a two-way repeated measures ANOVA with the Greenhouse-Geisser correction of memory field (left/right) and WM load (1/2/4/6).

2.7. Instantaneous frequency (IF) analysis

To validate the IPI analysis, we also computed the instantaneous frequency (Cohen, 2014; Wutz et al., 2018) of MEG data (**Fig. S6**). First, neuromagnetic signals at alpha-to-beta band (8–30 Hz) were isolated with the band-pass filter. Using the Hilbert transform, we converted the filtered waveform into changes in phase angle over time. The instantaneous frequency (IF) was obtained as the temporal derivative of this phase-angle time series (Cohen, 2014). Noises (sharp frequency jumps) in the IF waveforms were removed by a median filter with 11 equally-spaced time windows from 10 to 410 ms (Noguchi and Kubo, 2020).

It should be noted that the IF represents a speed of neural oscillation (a higher IF denotes faster oscillation). A statistical *t*-maps of IF (e.g. Memorize-Left vs. Memorize-Right) thus would be identical to those of mean IPI with signs of *t*-values reversed (because a shorter IPI is associated with higher IF).

3. Results

3.1. Behavioral data

Hit and FA rates of the change detection task were shown in **Fig. 2B**. Although the hit rate was above 90% in array sizes 1 (94.3 ± 1.2%, mean ± SE across participants) and 2 (91.6 ± 1.4%), it decreased to 69.4 ± 2.6% in size 4 and 50.5 ± 3.4% in size 6. The FA rate, on the other hand, increased monotonically as a function of WM load (size 1: 2.0 ± 0.5%, size 2: 3.6 ± 0.8%, size 4: 10.8 ± 1.8%, size 6: 15.9 ± 2.4%). Memory capacity *K* (right panel) estimated from those hit and FA rates were 0.92 ± 0.01 (load 1), 1.76 ± 0.04 (load 2), 2.34 ± 0.11 (load 4), and 2.07 ± 0.15 (load 6). A one-way repeated-measures ANOVA with the Greenhouse-Geisser correction on *K* indicated a significant main effect of WM load ($F(1.45,33.29) = 65.81$, $p < 0.001$, $\eta^2 = 0.741$). Post-hoc tests with the Bonferroni correction indicated significant differences in loads 1 vs. 2 ($p < 0.001$), 1 vs. 4 ($p < 0.001$), 1 vs. 6 ($p < 0.001$), and 2 vs. 4 ($p < 0.001$).

Consistent results were obtained in reaction time (RT) data measured from an onset of the test array. Means and SDs of RTs were 1185.6 ± 446.4 ms (load 1), 1241.5 ± 421.3 ms (load 2), 1357.5 ± 440.6 ms (load 4), and 1435.9 ± 497.4 ms (load 6). The one-way repeated-measures ANOVA yielded a significant main effect of WM load ($F(2.20,50.59) = 24.99$, $p < 0.001$, $\eta^2 = 0.521$), and post-hoc tests revealed significant differences in loads 1 vs. 4 (corrected $p = 0.0018$), 1 vs. 6 ($p < 0.001$), 2 vs. 4 ($p = 0.0081$), and 2 vs. 6 ($p < 0.001$).

We also found that a rate of "change" response in the catch trial was much lower (6.9 ± 1.2%, black dot in **Fig. 2B**) than the hit rate in load 2 (91.6%). This result indicates that participants correctly moved their attention into a left or right hemifield following the cue direction.

3.2. Changes in power of oscillatory signals during encoding and retention periods

Fig. 3B shows the time-frequency (TF) spectra at posterior sensors roughly over the occipito-parietal regions. In both hemispheres, we first observed an increase in power of theta band at 0 – 300 ms, which reflected the event-related fields of MEG signals, such as M100 and M170, elicited by a visual stimulus (memory array). Also prominent was a decrease in power of 8–30 Hz at 200 – 600 ms. This was followed by weak increase in alpha and beta powers after 600 ms. These results of power changes were consistent with previous studies on vWM (Erickson et al., 2019; Palva et al., 2011) and thus ensured the quality of present data.

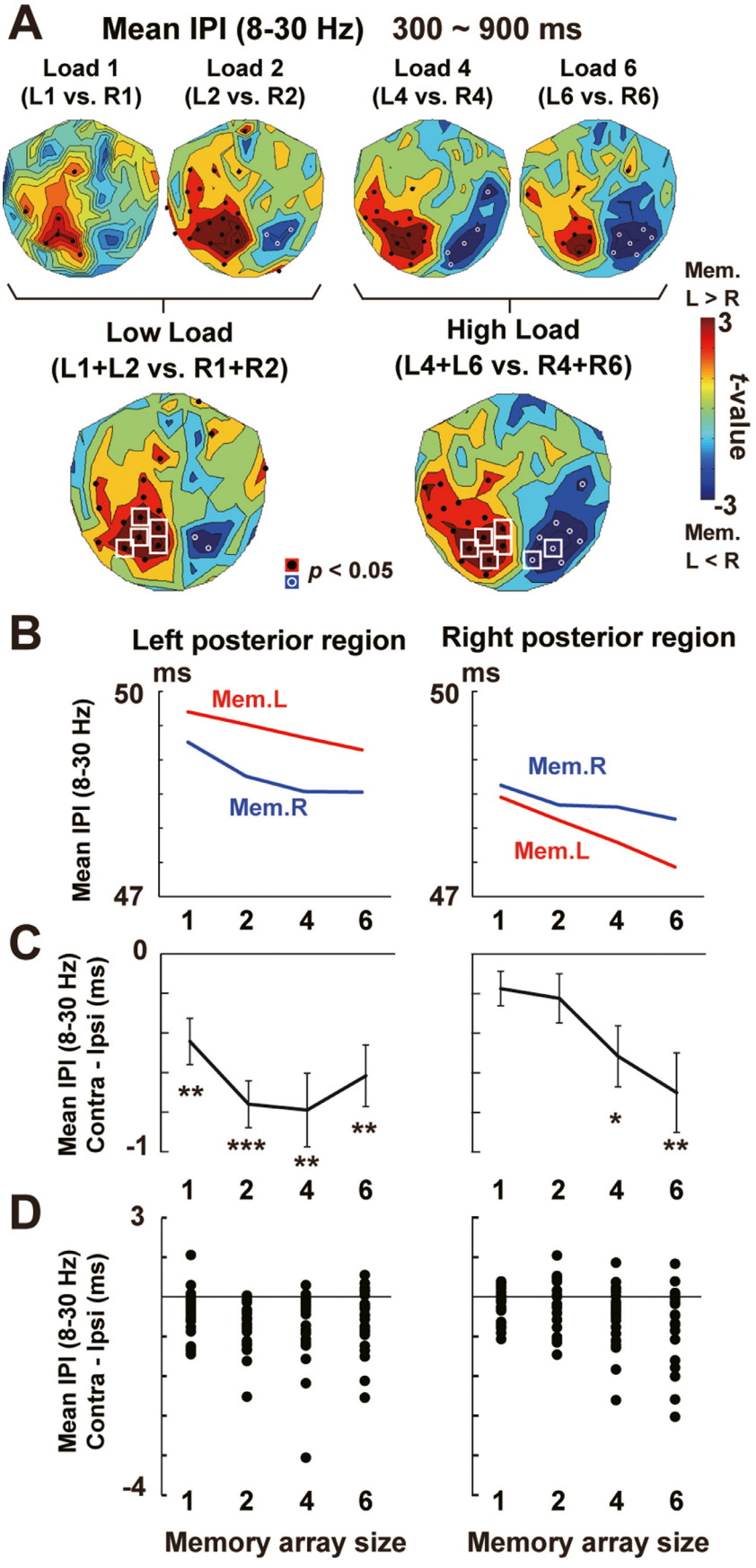

Fig. 5. Reduction of mean IPI as a function of memory load. (**A**) A comparison of Memorize-Left vs. Memorize-Right trials in each memory load. The maps in low-load conditions (1 and 2) and high-load conditions (4 and 6) are also shown in the lower panels. (**B**) Mean IPIs averaged across SOIs (see **Materials and Methods**) over the left occipito-parietal region (left panel) and right occipito-parietal region (right panel). At both hemispheres, a two-way ANOVA yielded significant main effects of memory field (left/right) and load (1/2/4/6). The right hemisphere further showed an interaction. (**C**) Differential IPIs. The IPIs became shorter when items in contralateral than ipsilateral hemifield were retained, and this difference grew larger as an increase in memory load (especially in the right hemisphere). These data indicate that changes in IPIs reflected memory, rather than attention or perception. Asterisks denote significant differences detected by post-hoc comparisons of the two-way ANOVA. $^{*}p < 0.05$, $^{**}p < 0.01$, $^{***}p < 0.001$ (**D**) Individual data of the differential IPIs.

3.3. Comparisons of IPIs between memorize-left and memorize-right conditions

Changes in IPIs related to WM maintenance were first explored by a contrast between Memorize-Left (L1-L6) and Memorize-Right (R1-R6) trials. The *t*-maps over the layout of 102 sensor positions (**Fig. 4B**) revealed that the posterior brain regions showed significant reductions of mean IPIs (8–30 Hz) when visual information in a contralateral hemifield was retained. As shown in **Fig. 5A**, this hemisphere-specific changes in IPIs became more evident in high-load conditions (4 and 6) than low-load conditions (1 and 2). Mean IPIs averaged across SOIs (see **Materials and Methods**) are displayed in **Fig. 5B-D**. At 6 SOIs in the left hemisphere, the two-way ANOVA of memory field (left/right) and WM load (1/2/4/6) indicated significant main effects of memory field ($F(1,23) = 36.93$, $p < 0.001$, $\eta^2 = 0.616$) and load ($F(1.66,38.16) = 13.92$, $p < 0.001$, $\eta^2 = 0.377$). No interaction, however, was observed ($F(3,69) = 1.89$, $p = 0.14$, $\eta^2 = 0.076$). On the other hand, 2 SOIs in the right hemisphere yielded significant main effects of memory field ($F(1,23) = 16.42$, $p < 0.001$, $\eta^2 = 0.416$) and load ($F(1.73,39.78) = 18.59$, $p < 0.001$, $\eta^2 = 0.447$) as well as their interaction ($F(3,69) = 3.91$, $p = 0.012$, $\eta^2 = 0.145$). Post-hoc comparisons of Memorize-Left vs. Memorize-Right for each load (with the Bonferroni correction) showed significant differences in load 4 (corrected $p = 0.011$) and load 6 ($p = 0.008$). Those data showed that the changes in mean IPIs reflected not only attention (main effect of memory field) and perception (main effect of array size) but also an amount of information stored in WM (interaction, the right hemisphere).

3.4. Effects of various factors on the relationships between IPIs and vWM

To validate the memory-related change in IPIs (**Fig. 4** and **Fig. 5**), we examined several factors that can affect results of IPI analysis. The first factor is time-dependent variables such as fatigue and shifts of head positions over time. In **Fig. S1**, we compared *t*-maps of mean IPIs (Memorize-Left vs. Memorize-Right) between the first and second halves of the experiment. Those maps showed consistent results; the hemisphere-specific and load-dependent changes of IPIs were observed throughout the experiment. The time-dependent variables therefore did not skew our results seriously.

The second factor was a time window for the IPI analysis (300 – 900 ms). As shown in **Fig. 3**, the alpha-to-beta band showed the prominent decrease in power before 600 ms but not after 600 ms. We thus compared *t*-maps between two time windows, one at 300 – 600 ms and the other at 600 – 900 ms. Consistent results were observed between the two windows (**Fig. S2**). Those data suggested that changes in IPIs continuously took place, although more prominent changes were seen in the first half (300 – 600 ms) than the second half (600 – 900 ms) of a retention interval.

Third, we performed the IPI analysis separately for alpha (8 – 12 Hz) and beta (13 – 30 Hz) bands, because a pass-band in **Figs. 4 and 5** had been wide (8 – 30 Hz). Results are shown in **Fig. S3**. In the low load condition, neither *t*-map of alpha nor beta band showed memory-related (hemisphere-specific) changes of IPIs. In the high-load condition, only *t*-map of beta band showed the hemisphere-specific changes, although they did not reach significance after the FDR correction. Therefore, the robust changes of IPIs both in low- and high-load conditions (**Fig. 5**) did not reflect either the alpha or beta rhythm but mainly emerged from an interplay of those two.

Fourth, while we had pooled the data of correctly-answered and incorrectly-answered trials in **Fig. 5**, they were separately analyzed in **Fig. S4**. We performed this analysis only for load 4 (L4 vs. R4) and load 6 (L6 vs. R6), because a number of incorrectly-answered trials were too small in low-load conditions (**Fig. 2B**). Memory-related changes in IPIs were more clearly seen in the correctly-answered than incorrectly-answered trials (**Fig. S4**).

Finally, we investigated IPIs by controlling for ages of participants. It has been shown that capacity of vWM shows age-related changes (Cowan et al., 2006; Sander et al., 2012), while participants over a broad age range were mixed in our sample. We thus re-analyzed IPIs by focusing on the data of 18 individuals in their 10 s or 20 s. As shown in **Fig. S5**, *t*-maps in this analysis were basically identical to those in **Fig. 5** ($N = 24$). Controlling for the age factor therefore did not affect our results.

3.5. Changes in instantaneous frequency related to vWM

To further validate the IPI analysis, we computed the instantaneous frequency (IF), an index for a speed of neural oscillation (a higher IF denotes faster oscillation). A comparison of Memorize-Left vs. Memorize-Right trials for each WM load was shown in **Fig. S6**. We found higher IF in the occipito-parietal regions when items in contralateral than ipsilateral hemifield were retained in memory. These results were consistent with **Fig. 5** showing memory-related decrease in IPIs.

3.6. Comparisons between high-K and low-K individuals

Previous studies reported substantial inter-individual differences in visual WM capacity (Cowan, 2001; Vogel et al., 2001); some people showed high *K* even in high-load conditions while others not. Can the IPI changes in alpha/beta band explain those inter-individual differences? We addressed this issue by dividing the 24 participants into two groups based on their *K*s averaged across all conditions (**Fig. 6A**). When mean IPIs in high-load conditions (L4, L6, R4, and R6) were compared with those in low-load conditions (L1, L2, R1, and R2), the high-*K* participants showed decreased IPIs (high-load < low-load) over a wide area of the brain (**Fig. 6B**, left). In contrast, this load-dependent reduction was observed only in posterior regions in the low-*K* participants (**Fig. 6B**, middle). A direct comparison of load effect (high-load minus low-load) between high- and low-*K* individuals revealed significant inter-group differences at anterior sensors roughly over the frontal cortex (**Fig. 6B**, right). As shown in **Fig. 6C**, the load-dependent reduction of the frontal IPIs was selectively seen in high-*K* subjects. We also observed a linear relationship ($r = -0.66$, $p < 0.001$) between IPI changes (high-load minus load-load) and *K* in high-load conditions (**Fig. 6D**).

Interestingly, the difference between high-*K* and low-*K* groups was also seen in IPIs during a baseline period, but in an opposite direction. **Fig. 7A** displays contour maps of mean IPIs in the baseline period (pre-cue period, from −1300 to −700 ms). The IPIs were longer in high-*K* than low-*K* individuals, indicating that higher task performance was associated with slower brain rhythms over the frontal cortex. When faced with high-load displays, high-*K* subjects memorized a large number of items by making their slow rhythm faster (solid lines in **Fig. 7B**). These data suggest that a key feature of high-*K* individuals was the changeability (flexibility) of brain rhythms, not a speed (absolute velocity) of oscillatory signals.

3.7. Memory-related changes in a variance of IPIs

We finally analyzed changes in variance of IPIs related to vWM. **Fig. 8** shows the CV (variance) of alpha/beta IPIs at 300 – 900 ms compared between Memorize-Left and Memorize-Right conditions. Smaller CVs denotes higher regularity of oscillatory signals. The CVs at right-hemisphere sensors became smaller when participant retained items in the left hemifield (colored in blue), whereas memorizing right-hemifield items reduced the variance at sensors over the left hemisphere (red). This pattern was most clearly observed in the low-load conditions of high-*K* participants.

4. Discussion

In the present study, we investigated changes in brain rhythms related to a retention of vWM. We found a load-dependent decrease in

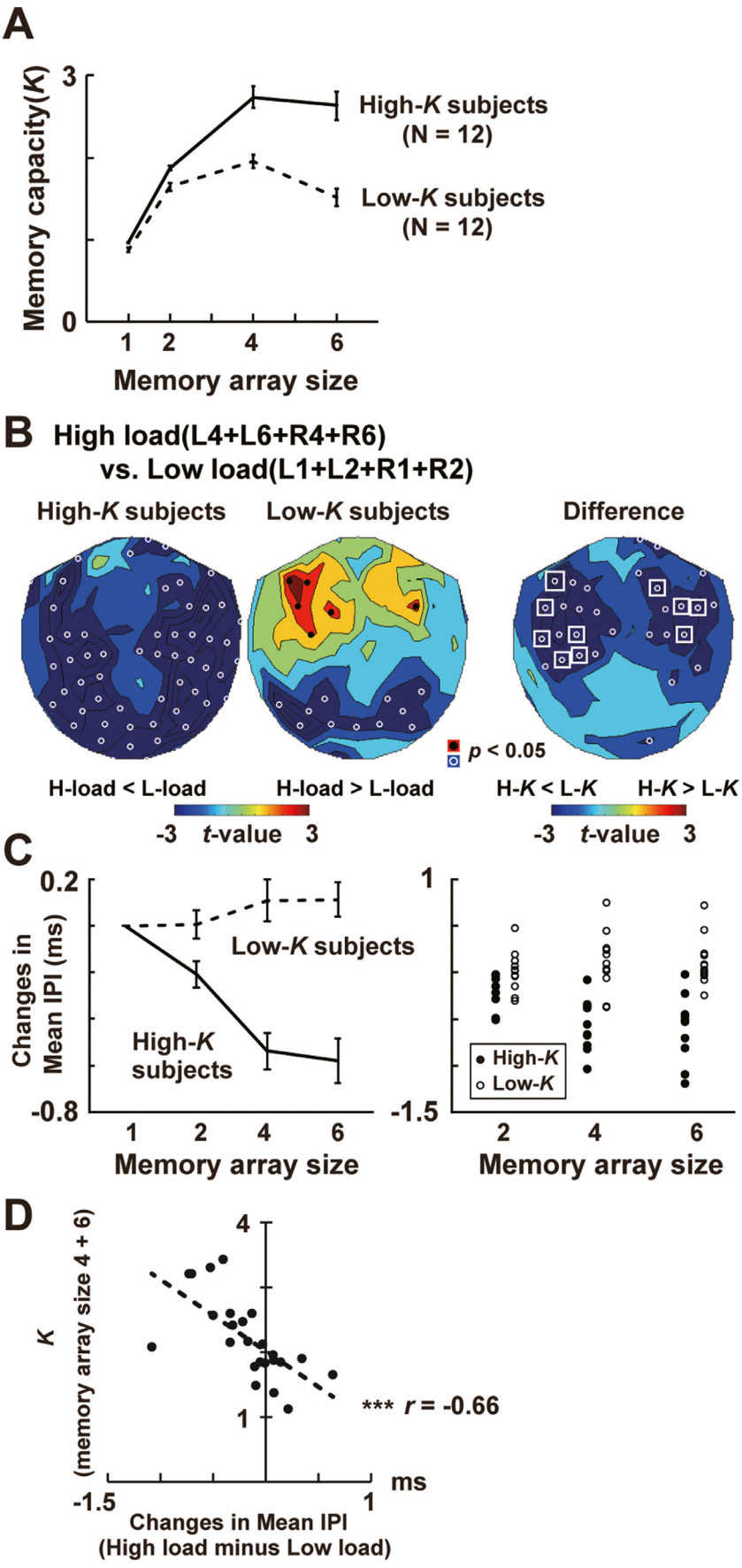

Fig. 6. Comparisons of high-*K* and low-*K* participants. (A) Memory capacity. The 24 participants were classified into high-*K* or low-*K* groups, based on their mean *K*s across four load levels. (B) The *t*-map of high-load (L4+L6+R4+R6) vs. low-load (L1+L2+R1+R2) conditions in high-*K* subjects (left panel) and low-*K* subjects (middle panel). Sensor positions showing shorter IPIs in high- than low-load conditions are shown in blue. In the right panel, differential IPIs (high-load minus low-load) are compared between high-*K* and low-*K* subjects (inter-group difference). High-*K* subjects were characterized by a load-dependent reduction of mean IPIs in anterior brain regions. (C) Changes in IPIs (left: mean ± SE, right: individual data) averaged across 10 sensors marked by white rectangles ($p < 0.05$, corrected) in panel B. Relative changes from load 1 condition are shown. (D) A correlation between IPI changes at the 10 sensors (high-load minus low-load) and *K* in high-load conditions of 24 participants. (For interpretation of the references to colour in this figure legend, the reader is referred to the web version of this article.)

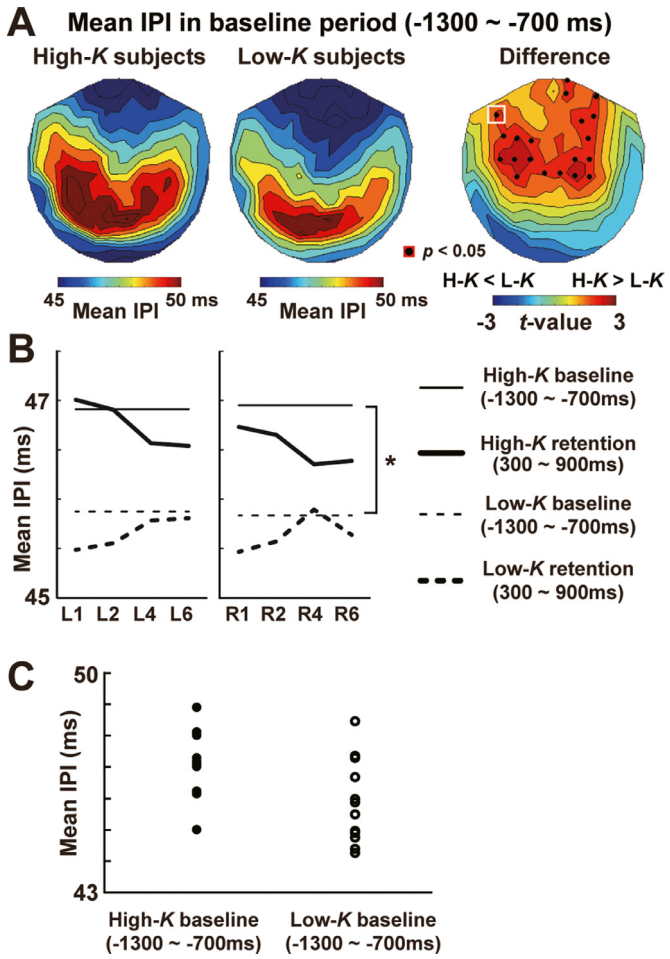

Fig. 7. Mean IPIs at 8 – 30 Hz during a baseline period (from −1300 to −700 ms). (A) Contour maps of baseline IPIs in high-*K* subjects (left), low-*K* subjects (middle), and an inter-group difference (*t*-map). The baseline IPIs were obtained as a mean across 8 conditions from L1 to R6. (B) IPIs in the retention (thick lines) and baseline (thin lines) periods of high-*K* (solid lines) and low-*K* subjects (dotted lines) at the left anterior sensor (white rectangle in panel A). High-*K* subjects were characterized by slower alpha-to-beta rhythm in the baseline period. When faced with high-load displays, they memorized a large number of items by making the slow rhythm faster. These data suggest that larger capacity was associated with greater changeability (flexibility) of brain rhythms. * $p < 0.05$ (C) Individual data of the baseline IPIs in high-*K* (filled dots) and low-*K* (open dots) subjects.

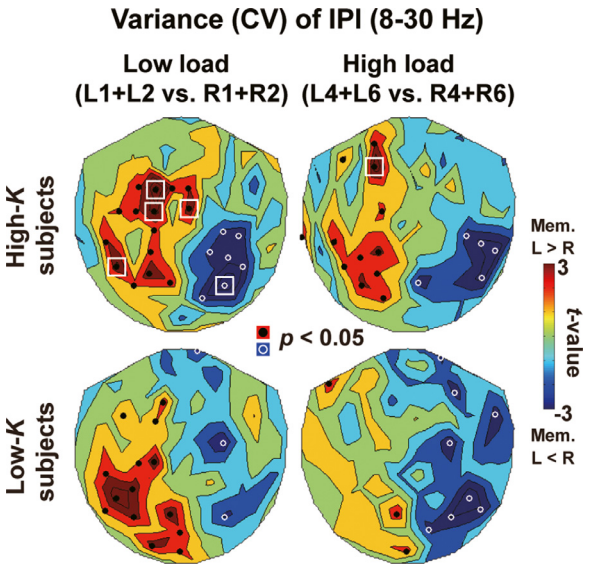

Fig. 8. Variance of IPIs during the retention period (300 – 900 ms). We computed the coefficients of variation (CVs), which was a standard deviation of IPIs divided by their mean (CV = SD/mean). Smaller CVs denotes smaller variance of IPIs (high regularity of oscillatory signals). Comparisons between Memorize-Left and Memorize-Right conditions reveal reduced CVs at sensors contralateral to a memory field, especially when high-*K* participants retained the information of low-load arrays (upper left). (For interpretation of the references to colour in this figure legend, the reader is referred to the web version of this article.)

mean IPIs over the occipito-parietal region contralateral to a memory field. A comparison between high-*K* and low-*K* participants further indicated a critical role of the anterior (frontal) regions in memorizing a large number of items simultaneously.

4.1. Reduction of mean IPIs and WM maintenance

Several studies have investigated a relationship between vWM and a speed of oscillatory signals in the fontal and parietal cortex. No consistent results, however, have been obtained so far. Using the Sternberg WM task, Babu Henry Samuel et al. (2018) measured a peak frequency of alpha rhythm (8–12 Hz) during a retention period of a digit set (e.g. 59713). They showed a negative correlation between oscillation frequency and behavioral data; trials with higher alpha frequency (faster rhythm) were associated with a lower performance of WM task (Babu Henry Samuel et al., 2018). Consistent with this view, Cohen (2011) investigated a peak frequency at 2–18 Hz in a retention period of a visual stimulus (line drawing), reporting that individuals with higher peak frequency showed lower performance in memory task (Cohen, 2011). In contrast, Moran et al. (2010) used the change detection task and reported that the peak frequency at 4–12 Hz was significantly higher in high capacity individuals than low capacity individuals (Moran et al., 2010). According to Moran et al. (2010), their data were consistent with the communication theory (Shannon, 1948) predicting a higher capacity of information transfer achieved by an increase in peak frequency.

Although it has been unclear what produced the mixed results in a previous literature, a hallmark of the present study was a measurement of IPIs at a wider bandwidth over alpha-to-beta range (8–30 Hz). This approach is based on a previous view that alpha and beta rhythms play a similar role in WM and thus can be seen as a unified band of oscillatory signals (Lundqvist et al., 2011; Miller et al., 2018; Roux and Uhlhaas, 2014). The mean IPIs identified with a pass band of 8–30 Hz actually showed clear decrease along with an increase in memory load (**Fig. 5**), which was associated with a better performance of WM task (**Fig. 6**). These results suggest that neural temporal codes related to WM are distributed in a broad frequency range over alpha to beta bands.

4.2. Inter-individual differences of mean IPIs in a baseline period

A comparison of high-*K* and low-*K* groups (**Fig. 6**) revealed that the high-*K* individuals showed a significant reduction of frontal IPIs in high-load conditions (L4, L6, R4, and R6) whereas the low-*K* individuals did not. It should be noted, however, that those results do *not* indicate a direct link between a faster brain rhythm and larger memory capacity, because high-*K* subjects showed a slower brain rhythm in a baseline period (**Fig. 7**). A key feature of high-*K* subjects therefore was the greater flexibility (changeability) of brain rhythms from low-load to high-load conditions. In previous studies, a successful maintenance of WM was associated with a high rate of neuronal firing in the prefrontal cortex (Constantinidis et al., 2018) or a formation of new patterns of brain rhythm, such as the cross-frequency coupling between theta and gamma waves (Lisman and Jensen, 2013). Our study proposes a new possibil-

ity that multi-item WM is achieved by a flexible modulation of ongoing brain rhythms in accordance with memory loads.

4.3. Reduced variance of IPIs in a retention period

We also found a significant decrease in variance of IPIs (increase in regularity of brain rhythms) during a retention interval (**Fig. 8**). Although several studies on human WM have analyzed regularity of neural activity using the correlation dimension (Grassberger and Procaccia, 1983), approximate entropy (Pincus, 1991) and Hurst exponent (Hurst, 1951), no consistent result has been obtained (Behzadfar et al., 2017; Zarjam et al., 2012). We presently approached this issue using the IPI analysis and found the memory-related increase in regularity. Our results support the attractor hypothesis in WM, because such attractor states are thought to emerge from self-sustained recurrent networks that can produce a periodic (regular) oscillatory signal.

Different from mean IPIs, the changes in regularity was more clearly observed in low- than high-load conditions (**Fig. 8**). Our behavioral data (**Fig. 2B**) showed that those low-load trials were characterized by higher hit rates and lower FA rates than high-load trials. The increased regularity of brain rhythm therefore might reflect a high fidelity of WM contents in those low-load trials.

4.4. Limitations

Finally, we refer to several limitations in the present study. The first limitation is a small number of participants (N = 24) and a distorted age distribution. Mounting evidence has shown that capacity of vWM shows age-related changes (Cowan et al., 2006; Sander et al., 2012). Recruiting a larger number of participants over a broader age range might reveal changes in IPI measures along with a development, providing further evidence for the relationship between IPIs and vWM. The second limitation is a lack of causal evidence. Although the alpha-to-beta IPIs were associated with individual vWM capacity (**Fig. 6** and **Fig. 7**), no evidence has been provided for a direct relationship between those two. A study using a causal approach, such as the transcranial alternating direct current stimulation (Wolinski et al., 2018), would resolve this issue. The third limitation is the unclarity of neural mechanisms for the memory-related changes of IPIs. The separate analysis of alpha (8 – 12 Hz) and beta (13 – 30 Hz) IPIs (**Fig. S3**) suggested that the present effects emerged from an interplay of alpha and beta rhythms, such as a phase-phase interaction of those two. Detailed mechanisms, however, remains unclear and thus should be examined carefully in future studies.

Declaration of competing interest

The authors declare no competing financial interest.

CRediT authorship contribution statement

Yasuki Noguchi: Conceptualization, Software, Investigation, Writing - original draft, Writing - review & editing. **Ryusuke Kakigi:** Supervision, Conceptualization, Writing - original draft, Writing - review & editing.

Acknowledgments

This work was supported by KAKENHI Grants Number 19H04430 from the Japan Society for the Promotion of Science (JSPS) to Y.N. We thank Mr. Y. Takeshima (National Institute for Physiological Sciences, Japan) for his technical supports. All data supporting the findings of this study are available from Y.N. upon reasonable request.

Supplementary materials

Supplementary material associated with this article can be found, in the online version, at doi:10.1016/j.neuroimage.2020.117294.

References

Axmacher, N., Henseler, M.M., Jensen, O., Weinreich, I., Elger, C.E., Fell, J., 2010. Cross-frequency coupling supports multi-item working memory in the human hippocampus. Proc Natl Acad Sci U S A 107, 3228–3233.
Babu Henry Samuel, I., Wang, C., Hu, Z., Ding, M., 2018. The frequency of alpha oscillations: task-dependent modulation and its functional significance. Neuroimage 183, 897–906.
Baddeley, A., 2012. Working memory: theories, models, and controversies. Annu Rev Psychol 63, 1–29.
Behzadfar, N., Firoozabadi, S.M.P., Badie, K., 2017. Analysis of regularity in the EEG before/after working memory task. In: 2017 24th National and 2nd International Iranian Conference on Biomedical Engineering (Icbme), pp. 213–217.
Benjamini, Y., Hochberg, Y., 1995. Controlling the False Discovery Rate - a Practical and Powerful Approach to Multiple Testing. J Roy Stat Soc B Met 57, 289–300.
Bonnefond, M., Jensen, O., 2012. Alpha oscillations serve to protect working memory maintenance against anticipated distracters. Curr Biol 22, 1969–1974.
Brainard, D.H., 1997. The Psychophysics Toolbox. Spat. Vis. 10, 433–436.
Brody, C.D., Romo, R., Kepecs, A., 2003. Basic mechanisms for graded persistent activity: discrete attractors, continuous attractors, and dynamic representations. Curr Opin Neuro. 13, 204–211.
Canolty, R.T., Edwards, E., Dalal, S.S., Soltani, M., Nagarajan, S.S., Kirsch, H.E., et al., 2006. High gamma power is phase-locked to theta oscillations in human neocortex. Science 313, 1626–1628.
Chaudhuri, R., Fiete, I., 2016. Computational principles of memory. Nat Neurosci 19, 394–403.
Cohen, M.X., 2011. Hippocampal-prefrontal connectivity predicts midfrontal oscillations and long-term memory performance. Curr Biol 21, 1900–1905.
Cohen, M.X., 2014. Fluctuations in oscillation frequency control spike timing and coordinate neural networks. J Neurosci 34, 8988–8998.
Compte, A., Brunel, N., Goldman-Rakic, P.S., Wang, X.J., 2000. Synaptic mechanisms and network dynamics underlying spatial working memory in a cortical network model. Cereb Cortex 10, 910–923.
Compte, A., Constantinidis, C., Tegner, J., Raghavachari, S., Chafee, M.V., Goldman-Rakic, P.S., et al., 2003. . Temporally irregular mnemonic persistent activity in prefrontal neurons of monkeys during a delayed response task. J Neurophysiol 90, 3441–3454.
Constantinidis, C., Funahashi, S., Lee, D., Murray, J.D., Qi, X.L., Wang, M., et al., 2018. Persistent Spiking Activity Underlies Working Memory. J Neurosci 38, 7020–7028.
Cowan, N., 2001. The magical number 4 in short-term memory: a reconsideration of mental storage capacity. Behav Brain Sci 24, 87–114 discussion 114-185.
Cowan, N., Naveh-Benjamin, M., Kilb, A., Saults, J.S., 2006. Life-span development of visual working memory: when is feature binding difficult? Dev Psychol 42, 1089–1102.
D'Esposito, M., Postle, B.R., 2015. The cognitive neuroscience of working memory. Annu Rev Psychol 66, 115–142.
Erickson, M.A., Smith, D., Albrecht, M.A., Silverstein, S., 2019. Alpha-band desynchronization reflects memory-specific processes during visual change detection. Psychophysiology 56, e13442.
Eriksson, J., Vogel, E.K., Lansner, A., Bergstrom, F., Nyberg, L., 2015. Neurocognitive Architecture of Working Memory. Neuron 88, 33–46.
Faul, F., Erdfelder, E., Lang, A.G., Buchner, A., 2007. G*Power 3: a flexible statistical power analysis program for the social, behavioral, and biomedical sciences. Behav Res Methods 39, 175–191.
Fukuda, K., Mance, I., Vogel, E.K., 2015. alpha Power Modulation and Event-Related Slow Wave Provide Dissociable Correlates of Visual Working Memory. J Neurosci 35, 14009–14016.
Gelastopoulos, A., Whittington, M.A., Kopell, N.J., 2019. Parietal low beta rhythm provides a dynamical substrate for a working memory buffer. Proc Natl Acad Sci U S A 116, 16613–16620.
Grassberger, P., Procaccia, I., 1983. Measuring the Strangeness of Strange Attractors. Physica D 9, 189–208.
Hurst, H.E., 1951. Long-Term Storage Capacity of Reservoirs. T Am Soc Civ Eng 116, 770–799.
Inagaki, H.K., Fontolan, L., Romani, S., Svoboda, K., 2019. Discrete attractor dynamics underlies persistent activity in the frontal cortex. Nature 566, 212–217.
Jacob, S.N., Hahnke, D., Nieder, A., 2018. Structuring of Abstract Working Memory Content by Fronto-parietal Synchrony in Primate Cortex. Neuron 99, 588–597 e585.
Jensen, O., Gelfand, J., Kounios, J., Lisman, J.E., 2002. Oscillations in the alpha band (9-12 Hz) increase with memory load during retention in a short-term memory task. Cereb Cortex 12, 877–882.
Jensen, O., Mazaheri, A., 2010. Shaping functional architecture by oscillatory alpha activity: gating by inhibition. Front Hum Neurosci 4, 186.
Johnson, E.L., Dewar, C.D., Solbakk, A.K., Endestad, T., Meling, T.R., Knight, R.T., 2017. Bidirectional Frontoparietal Oscillatory Systems Support Working Memory. Curr Biol 27, 1829–1835 e1824.
Kaminski, J., Sullivan, S., Chung, J.M., Ross, I.B., Mamelak, A.N., Rutishauser, U., 2017. Persistently active neurons in human medial frontal and medial temporal lobe support working memory. Nat Neurosci 20, 590–601.
Kornblith, S., Buschman, T.J., Miller, E.K., 2016. Stimulus Load and Oscillatory Activity in Higher Cortex. Cereb Cortex 26, 3772–3784.

Leavitt, M.L., Mendoza-Halliday, D., Martinez-Trujillo, J.C., 2017. Sustained Activity Encoding Working Memories: not Fully Distributed. Trends Neurosci 40, 328–346.
Lisman, J.E., Jensen, O., 2013. The theta-gamma neural code. Neuron 77, 1002–1016.
Luck, S.J., Vogel, E.K., 2013. Visual working memory capacity: from psychophysics and neurobiology to individual differences. Trends Cogn Sci 17, 391–400.
Lundqvist, M., Herman, P., Lansner, A., 2011. Theta and gamma power increases and alpha/beta power decreases with memory load in an attractor network model. J Cogn Neurosci 23, 3008–3020.
Lundqvist, M., Herman, P., Miller, E.K., 2018. Working Memory: delay Activity, Yes! Persistent Activity? Maybe Not. J Neurosci 38, 7013–7019.
Ma, W.J., Husain, M., Bays, P.M., 2014. Changing concepts of working memory. Nat Neurosci 17, 347–356.
Macoveanu, J., Klingberg, T., Tegner, J., 2006. A biophysical model of multiple-item working memory: a computational and neuroimaging study. Neuroscience 141, 1611–1618.
Mapelli, I., Ozkurt, T.E., 2019. Brain Oscillatory Correlates of Visual Short-Term Memory Errors. Front Hum Neurosci 13, 33.
Miller, E.K., Lundqvist, M., Bastos, A.M., 2018. Working Memory 2.0. Neuron 100, 463–475.
Moran, R.J., Campo, P., Maestu, F., Reilly, R.B., Dolan, R.J., Strange, B.A., 2010. Peak frequency in the theta and alpha bands correlates with human working memory capacity. Front Hum Neurosci 4, 200.
Murray, J.D., Bernacchia, A., Roy, N.A., Constantinidis, C., Romo, R., Wang, X.J., 2017. Stable population coding for working memory coexists with heterogeneous neural dynamics in prefrontal cortex. Proc Natl Acad Sci U S A 114, 394–399.
Noguchi, Y., Kubo, S., 2020. Changes in latency of brain rhythms in response to affective information of visual stimuli. Biol Psychol 149, 107787.
Noguchi, Y., Xia, Y., Kakigi, R., 2019. Desynchronizing to be faster? Perceptual- and attentional-modulation of brain rhythms at the sub-millisecond scale. Neuroimage 191, 225–233.
Palva, S., Kulashekhar, S., Hamalainen, M., Palva, J.M., 2011. Localization of cortical phase and amplitude dynamics during visual working memory encoding and retention. J Neurosci 31, 5013–5025.
Pashler, H., 1988. Familiarity and visual change detection. Percept Psychophys 44, 369–378.
Pelli, D.G., 1997. The VideoToolbox software for visual psychophysics: transforming numbers into movies. Spat. Vis. 10, 437–442.
Pincus, S.M., 1991. Approximate entropy as a measure of system complexity. Proc Natl Acad Sci U S A 88, 2297–2301.
Proskovec, A.L., Wiesman, A.I., Heinrichs-Graham, E., Wilson, T.W., 2018. Beta Oscillatory Dynamics in the Prefrontal and Superior Temporal Cortices Predict Spatial Working Memory Performance. Sci Rep 8, 8488.
Qi, X.L., Constantinidis, C., 2015. Lower neuronal variability in the monkey dorsolateral prefrontal than posterior parietal cortex. J. Neurophysiol 114, 2194–2203.
Reinhart, R.M.G., Nguyen, J.A., 2019. Working memory revived in older adults by synchronizing rhythmic brain circuits. Nat Neurosci 22, 820–827.
Roux, F., Uhlhaas, P.J., 2014. Working memory and neural oscillations: alpha-gamma versus theta-gamma codes for distinct WM information? Trends Cogn Sci 18, 16–25.
Sander, M.C., Lindenberger, U., Werkle-Bergner, M., 2012. Lifespan age differences in working memory: a two-component framework. Neurosci Biobehav Rev 36, 2007–2033.
Sauseng, P., Klimesch, W., Heise, K.F., Gruber, W.R., Holz, E., Karim, A.A., et al., 2009. . Brain oscillatory substrates of visual short-term memory capacity. Curr Biol 19, 1846–1852.
Shannon, C.E., 1948. A Mathematical Theory of Communication. Bell Syst Tech J 27, 379–423.
Shin, H., Law, R., Tsutsui, S., Moore, C.I., Jones, S.R., 2017. The rate of transient beta frequency events predicts behavior across tasks and species. Elife 6.
Spitzer, B., Haegens, S., 2017. Beyond the Status Quo: a Role for Beta Oscillations in Endogenous Content (*Re*)Activation. eNeuro 4.
Standage, D., Pare, M., 2018. Slot-like capacity and resource-like coding in a neural model of multiple-item working memory. J Neurophysiol 120, 1945–1961.
Stokes, M.G., 2015. 'Activity-silent' working memory in prefrontal cortex: a dynamic coding framework. Trends Cogn Sci 19, 394–405.
Tadel, F., Baillet, S., Mosher, J.C., Pantazis, D., Leahy, R.M., 2011. Brainstorm: a user-friendly application for MEG/EEG analysis. Comput Intell Neurosci 2011, 879716.
van Ede, F., de Lange, F., Jensen, O., Maris, E., 2011. Orienting attention to an upcoming tactile event involves a spatially and temporally specific modulation of sensorimotor alpha- and beta-band oscillations. J Neurosci 31, 2016–2024.
Vogel, E.K., Machizawa, M.G., 2004. Neural activity predicts individual differences in visual working memory capacity. Nature 428, 748–751.
Vogel, E.K., Woodman, G.F., Luck, S.J., 2001. Storage of features, conjunctions and objects in visual working memory. J Exp Psychol Hum Percept Perform 27, 92–114.
Wianda, E., Ross, B., 2019. The roles of alpha oscillation in working memory retention. Brain Behav 9, e01263.
Wimmer, K., Nykamp, D.Q., Constantinidis, C., Compte, A., 2014. Bump attractor dynamics in prefrontal cortex explains behavioral precision in spatial working memory. Nat Neurosci 17, 431–439.
Wolinski, N., Cooper, N.R., Sauseng, P., Romei, V., 2018. The speed of parietal theta frequency drives visuospatial working memory capacity. PLoS Biol 16, e2005348.
Wutz, A., Melcher, D., Samaha, J., 2018. Frequency modulation of neural oscillations according to visual task demands. Proc Natl Acad Sci U S A 115, 1346–1351.
Zarjam, P., Epps, J., Lovell, N.H., Chen, F., 2012. Characterization of memory load in an arithmetic task using non-linear analysis of EEG signals. Conf Proc IEEE Eng Med Biol Soc 2012, 3519–3522.